Post-stenotic flow in an artery

T. J. Barber[1], E. Jarratt[1], K. Kabir[1], A. Simmons[1]

[1]School of Mechanical and Manufacturing Engineering, The University of New South Wales, New South Wales 2052, Australia
t.barber@unsw.edu.au

Abstract

Computational fluid dynamics simulation of stenosed arteries, combined with ex-vivo measurement for validation, allows the analysis of fluid dynamic quantities that are difficult to measure in an in-vivo environment. The analysis of fluid dynamics properties such as wall shear stress, velocity, viscosity and pressure is important in understanding the likely causes and ongoing effects of stenosis. In this study, a three-dimensional computational fluid dynamics simulation is conducted of a representative stenosed artery [5]. A physiological inlet condition, representing a femoral artery, is used as the transient inlet condition. Concurrently, an experimental study is conducted of the identical geometry, and laser sheet visualization is used with a continuous Nd-YAG laser to highlight regions of the flowfield, including the post-stenotic jet core field, and the associated recirculation regions. Due to the retrograde flow for a section of the pulsatile profile, a core region surrounded by recirculation regions is also found proximal to the stenosis. High values of wall shear stress and oscillatory values of wall shear stress (varying in both space and time) are observed, which are indicators of possible future cell damage.

Introduction

Arterial disease can result in stenosis, in which there is a narrowing of the artery, resulting in a smaller area for the blood to flow through. This —sometimes dramatic— change in cross-sectional area can cause significant changes to the blood flow, including the presence of a jet in the region downstream (distal) to the stenosis and large changes in wall shear stress when the corresponding shear layer breaks up. The further complication of pulsatile flow results in a challenging fluid dynamics problem and much of the previous work in stenosed arterial flow has made use of steady state conditions, or non-physiological inlet profiles such as sine waves. Analysis of vascular fluid dynamic quantities such as velocity profiles, turbulent quantities and associated wall shear stress (WSS) are important in gaining an understanding of the mechanisms that may contribute to conditions such as atherosclerosis. However, in vivo measurement of these data is difficult; computational modelling and experimental simulation are proving to be useful methods for gaining such information. Berger and Lou [4], in their comprehensive review of stenotic vessel flows, note that studies of WSS have been the motivation behind much of the work in this area in recent decades. While regions of both high and low shear stress have been highlighted as potential atherosclerotic development sites, it is now accepted that how rapidly the WSS varies in space and time is of significance. Fluid shear stresses in healthy large arteries is typically 1-2 Pa [4], however may be as large as 200Pa in the narrowed throat region of a severely stenosed artery [7].

Khalifa [6] identified three distinct types of post-stenotic flow disturbances. The first is an obvious 'start-up structure' that corresponds to the beginning of each flow cycle. It results from a new 'slug' of fluid passing through the constriction, and is visible in stenoses as mild as 25% area reduction. The second type of disturbance occurs in stenoses with 50% area reduction or more, and is a form of shear layer oscillation, or vortex shedding, that occurs as the shear layer becomes unstable and starts to 'roll up' into vortices [9]. The third form of disturbance identified is the decay of the shear layer oscillation into turbulence further downstream.

It has been shown that under the pressure conditions found in a human artery, the cross-section of the stenosis is often axisymmetric, rather than asymmetric [1]. The contour of the stenosis profile also tends to be smooth as a result of platelet deposition. Siouffi [8] developed a representative geometry based on the exponential function and it is this geometry that has been used in the current work to represent a stenosed femoral artery:

$$\frac{R(z)}{R_0} = 1 - 0.5\exp\left(-\frac{4z^2}{R_0^2}\right) \qquad (1)$$

The femoral artery was selected due to the prevalence of stenosis and also due to the reversing nature of the flow profile. This flow reversal creates an interesting problem, both experimentally and computationally, and presents a number of interesting flow features.

Dynamically similar models are developed experimentally and computationally and an examination is made of the flow characteristics and their significance.

Experimental method

Pulsatile arterial flow is governed by two non-dimensional parameters, the Reynolds number:

$$Re = \frac{\rho \bar{V} D}{\mu} = \frac{\bar{V} D}{\nu} \qquad (2)$$

and the Womersley parameter:

$$\alpha = \frac{D}{2}\sqrt{\frac{\rho \omega}{\mu}} = \frac{D}{2}\sqrt{\frac{\omega}{\nu}} \qquad (3)$$

where ρ is the density of the fluid under consideration, $\bar{V}$ is the average velocity of the fluid, D is the diameter of the pipe through which the fluid flows, μ is the dynamic viscosity of the fluid, ν is the kinematic viscosity of the fluid and ω is the angular frequency of oscillations in the fluid.

In order to gain reasonable experimental data, using Re and α the geometry has been scaled from a typical femoral artery diameter of 10 mm to an experimental model diameter of 31.7 mm. From consideration of the typical rheological properties of blood, the mean diameter of 9.8 mm for the femoral artery, and a mean velocity of 0.12 m/s for blood in the femoral artery, the mean Reynolds number for the femoral artery is found to be 274. In order to retain dynamic similarity, the pulsatile inlet profile period has increased from a real life situation of 0.6 s to

28.14 s (see Figure 1). Computational models are set to replicate as closely as possible the experiment: the same size and geometrical profile were used and the experimentally measured velocity profile was used as the computational inlet.
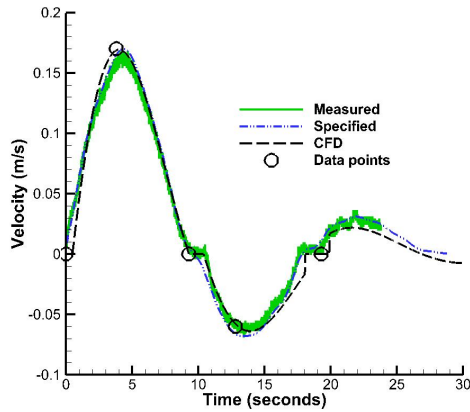

Figure 1: Femoral artery flow profiles use in the present study

A schematic of the experimental rig is shown in Figure 2. It comprises a computer-controlled flow pump system with an associated fluid reservoir, connected to the stenosis test section by means of semi-rigid and rigid acrylic tubing, as well as four acrylic blocks; two blocks serve as end sections that connect the rigid acrylic pipe to two other blocks with uniform internal diameter. The actual stenosis section was NC-milled from cast acrylic. The CardioFlow pump is a computer-controlled physiological flow pump that can generate repeatable flow profiles over a flow range of 50 mL/s to 300 mL/s. It comprises a pump unit, an external reservoir and a control unit. Due to the mechanical nature of the pump, the actual (measured) flow profile varies from that specified, as shown in Figure1. Using a EMPCO Blood Flow Transducer, the profile was measured just prior to the test section and a Fourier transform was used to decompose the data into a set of five equations which were then used an input to the CFD model.
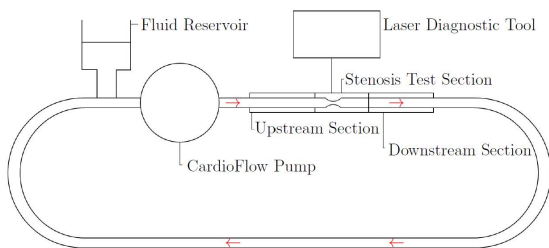

Figure 2: Schematic of experimental rig [2].

To gain accurate data from the optical measurement techniques, the refractive index (RI) of the fluid and the test section material needed to be matched. It was also necessary to match, to some extent, the viscosity of the test fluid to that of blood, to both simulate blood flow and to lubricate the pump. The optimum solution was found to be 65.5% NaI with 20% glycerol.The density of the test fluid was also measured several times and found to be 1665 kgm^{-3}, giving the dynamic viscosity of the test fluid as 0.00582 Ns/m^2. The calculated values for mean flow rate and period for the fluid in the rig are $Q_m = 17.1$ mL/s for $Re_m = 274$ and $T = 39.5$ s, $\alpha = 4$ and the minimum hydrodynamic entry length required for developed flow is 0.652 m.

Laser sheet flow visualisation is a technique that involves introducing seeding particles with a similar density to the working fluid, upstream of the area of interest of the flow. A thin sheet of laser light — approximately 1.5 mm in thickness — is placed in the centre of the flow, parallel to the flow in the plane of interest, and a camera takes a photograph or video of the particles as the laser light sheet illuminates them. The present study uses a 125 mW Nd:YAG laser that produces a beam of light with a wavelength of 532 nm, which appears as bright green. A cylindrical optical lens turns this beam into a laser sheet, and the laser itself is held above the stenosis test section by means of a precision stand. The fluid is seeded with 5 μm polyamide particles at a concentration of approximately 3 mg/L. The images of the flow are captured with a Nikon D5100 digital SLR camera with a 105 mm lens, and the aperture and exposure time set to f/3.5 and 1/13s respectively. Post-processing of the images is required, including converting the image to black and white and increasing the contrast.

Computational model

The geometry consists of an exact model of the experimental stenosis test section, and the modelled region extends 15D before the stenosis begins, and extends 15D beyond the stenosis. The flow is assumed to be incompressible, homogenous and Newtonian with the fluid properties set to the fluid used in the experimental model. The vessel walls are assumed rigid. The assumption of rigid walls is common; atherosclerosis is likely to reduce elasticity in the vessel walls and Newtonian flow in vessels of this size has been shown to be a reasonable assumption. The inlet conditions were set as plug flow (e.g uniform across the boundary); a parabolic, fully developed profile is not appropriate for velocity conditions that may experience flow reversal. The experimentally measured profile is used as the inlet profile, via a User Defined Function using a five-part equation. All vessel walls are set to non-slip boundaries and the downstream outlet is an open boundary that allows both forward and reverse flow. A fully structured mesh was produced using ANSYS ICEM, with mild bias towards the walls to enable capture of boundary layer development and also mild bias from both the inlet and outlet towards the region of the stenosis. The mesh consisted of 15 blocks of structured hexahedral cells, giving a total number of cells of 750,000. A timestep of 0.01 s was used and the residual error level within each timestep, for each equation, was $1x10^{-5}$. The residual error was determined by considering the variation of axial velocity at a number of points within the flow field. All cases were run with double-precision accuracy. The Reynolds Averaged Navier Stokes equations are solved using a commercial finite volume code, ANSYS Fluent 13.0.0. Momentum equations were solved by QUICK discretization and pressure-velocity coupling was achieved with the SIMPLEC scheme. Turbulence may be found in the post-stenotic region of the flow and therefore the SST k-ω model for turbulence closure was applied. Six full pulsatile cycles were completed before the collection of data, allowing the flow to settle and relevant flow parameters to reach consistent values between each cycle.

Results

In order to first explain the flow conditions apparent for this situation, CFD results are presented for the axial flow along a midplane (Figure 3). Contour plots are given at five key points in the cycle (see Figure 1) in order to capture the transient nature of the flow. At t = 3.8 s, the cycle is near peak systole and a reasonably uniform flow can be observed, with a central core of high-speed fluid moving downstream of the stenosis, surrounded by sections of slow reverse (negative x direction) flow. The core is well-contained and extends approximately 3D
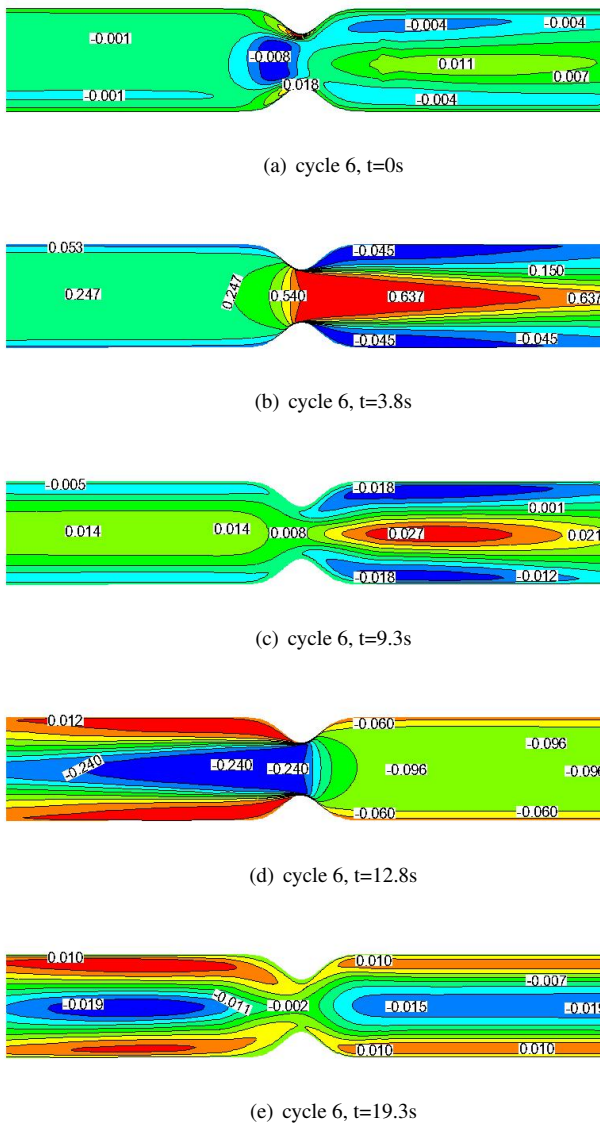
(a) cycle 6, t=0s

(b) cycle 6, t=3.8s

(c) cycle 6, t=9.3s

(d) cycle 6, t=12.8s

(e) cycle 6, t=19.3s

Figure 3: Axial velocity (ms^{-1}) on mid-plane over the cycle

(a) cycle 6, t=0s

(b) cycle 6, t=3.8s

(c) cycle 6, t=9.3s

(d) cycle 6, t=12.8s

(e) cycle 6, t=19.3s

Figure 4: Flow field using CFD (left) and laser sheet flow visualization (right) on mid-plane over the cycle

from the stenosis. At t = 9.3 s the inlet has slowed to zero flow, and while some remnant of the core flow can be seen the majority of the fluid has decreased in velocity. At t = 12.8 s, the cycle has reached peak diastole, and most of the fluid is moving in the reverse direction. Again, a core of fast-moving fluid is observed (now on the left side of the stenosis). Regions of recirculating fluid are seen on either side of the core and downstream of the stenosis. At t = 19.3 s, the inlet has again slowed to a zero point and this is apparent in the decreased velocity across the flow field. Again, the remnant of the core flow can be seen to the left of the stenosis. A small amount of reversed flow remains upstream of the stenosis, where the fast-moving core existed at the earlier time-step.

Considering now the experimental results and analysing the flow structures in more detail, images are presented of flow visualization for the downstream region of the stenosis. For comparison, CFD data is presented on the left of each figure, as vectors and streamtraces. At t = 0 s, the start-up structure is apparent, followed by the first vortices, which quickly cause an oscillating shear layer of small, coherent vortices to form. A smoother flow field is observed in the computational results,
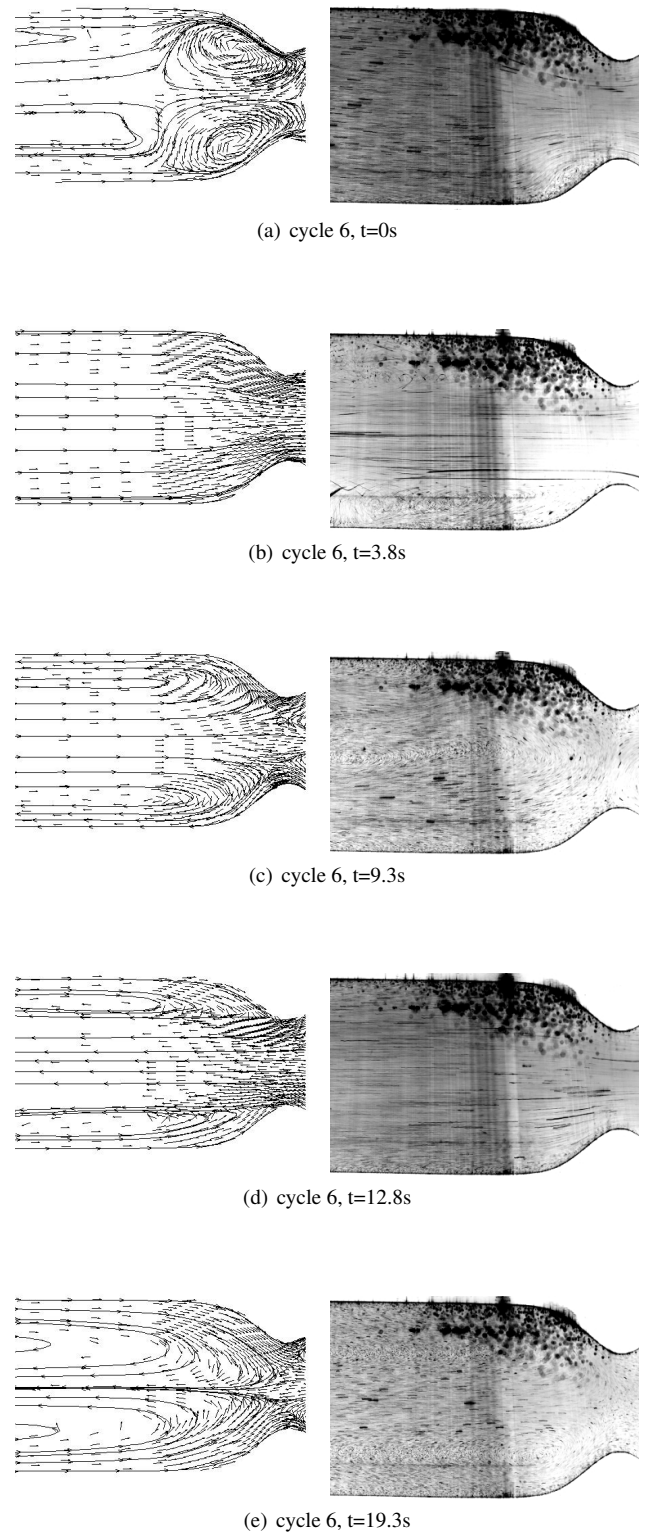
due to the Reynolds Averaged solution process. This shear layer grows thicker during the acceleration phase of the flow cycle until the point of peak flow at t = 3.8 s, when the shear layer has broken up and dissolved into random flow, beginning at one to two diameters downstream of the throat of the stenosis. As the
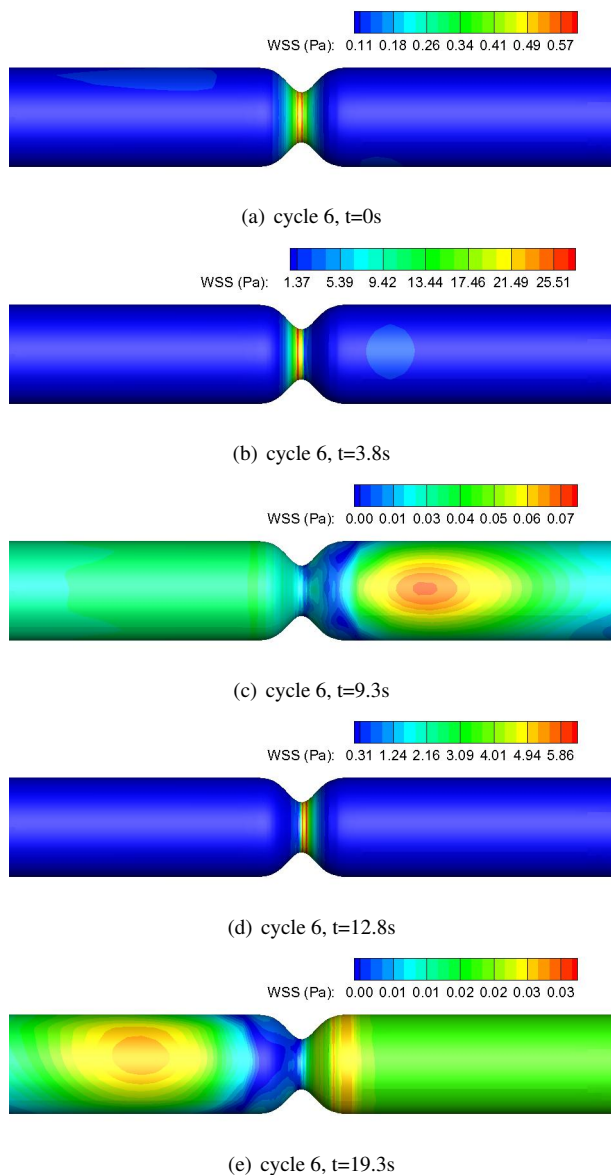
(a) cycle 6, t=0s

(b) cycle 6, t=3.8s

(c) cycle 6, t=9.3s

(d) cycle 6, t=12.8s

(e) cycle 6, t=19.3s

Figure 5: Wall shear stress (Pa) on the wall over the cycle (note local contour ranges)

upstream flow becomes zero, at t = 9.3 s the fluid slowly circulates distal to the stenosis. At the point of zero upstream flow the only obvious flow characteristic is that the velocity values distal to the stenosis, although they are very small, are not zero. This is due to the inertia of the fluid, which has formed several slowly circulating vortices distal to the stenosis. The characteristics of the fluid at the point of zero upstream flow is an important factor in assessing the coherency of the post-stenotic flow. As the flow reverses at t = 12.8 s, a central core region is seen with recirculating regions of fluids to either side. It is this type of dramatic change in boundary layer fluid flow that creates high levels of oscillatory shear stress; a known cause of damage to the cells lining the vessel wall. As a positive flow is once again imposed upstream of the stenosis, the jet at the centre of the artery is still travelling with a negative velocity. The fluid flowing in the positive direction shown for t = 19.3 s is not fast enough to overcome the inertia of the fluid with this negative velocity, and so at first, it 'wraps around' the jet at the centre, creating vortices in the fluid on either side of the jet.

Finally, the computational results allow analysis of the wall

shear structure, which is difficult to measure experimentally. Figure 5 is a representation of the wall shear stress (WSS) on the wall, at the key times in the cycle. Due to the large variations in WSS, each image has it own range of contour level and legend. As expected, elevated levels of WSS are found in the stenosis, where the fluid velocity is greatest and forced through a narrow region. It is interesting to note the very high levels found for the peak flow at t = 3.8 s, where greater than 25 Pa are seen. As noted earlier, low and also oscillatory WSS are also indicators of possible cell damage, and the variation of WSS over space and through time is clearly indicated in Figure 5. Some three-dimensionality is also noted in the WSS results; previous work using Large Eddy Simulation has found evidence of significant three-dimensionality for stenosed artery flows [3]. The pulsatile, and particularly reverse flow found for the femoral artery, produces large variations in WSS. At t = 9.3 s and t = 19.3 s regions of WSS variation are seen on the vessel wall where the shear layer breakup is apparent.

Conclusions

Computational and experimental analyses were conducted for the case of a representative femoral artery, with a physiological flow profile. Laser sheet flow visualization images and analysis of the computational results demonstrated the complex flow structures present, including a central core flow that is present on either side of the stenosis for different points during the cycle. Wall shear stresses, found computationally, were seen to vary significantly, both temporally and spatially indicating the likely occurrence of further cell damage.

*

References

[1] Ahmed, S. A. and Giddens, D. P., Pulsatile poststenotic flow studies with laser Doppler anemometry, *Journal of Biomechanics*, **17**, 1984, 695–705.

[2] Barber, T., Jarratt, E. and Simmons, A., Considerations for the development of an optically accessible stenosed artery experiment, in *Proceedings of the 6th Australian Conference on Laser Diagnostics in Fluid Mechanics and Combustion*, Canberra, Australia, 2011.

[3] Barber, T. J. and Simmons, A., Large eddy simulation of a stenosed artery using a femoral artery pulsatile flow profile, *Artificial Organs*, **35**, 2011, E155–E160.

[4] Berger, S. A. and Jou, L.-D., Flows in Stenotic Vessels, *Annual Review of Fluid Mechanics*, **32**, 2000, 347–382.

[5] Deplano, V. and Siouffi, M., Experimental and numerical study of pulsatile flows through stenosis::: Wall shear stress analysis, *Journal of Biomechanics*, **32**, 1999, 1081–1090.

[6] Khalifa, A. M. A. and Giddens, D. P., Characterization and evolution poststenotic flow disturbances., *Journal of Biomechanics*, **14**, 1981, 279–96.

[7] Li, M., Beech-Brandt, J., John, L., Hoskins, P. and Easson, W., Numerical analysis of pulsatile blood flow and vessel wall mechanics in different degrees of stenoses, *Journal of biomechanics*, **40**, 2007, 3715–3724.

[8] Siouffi, M., Pélissier, R., Farahifar, D. and Rieu, R., The effect of unsteadiness on the flow through stenoses and bifurcations, *Journal of Biomechanics*, **17**, 1984, 299–315.

[9] Varghese, S. S., Frankel, S. H. and Fischer, P. F., Direct numerical simulation of stenotic flows. Part 2. Pulsatile flow, *Journal of Fluid Mechanics*, **582**, 2007, 281–318.